Nuclear Inst. and Methods in Physics Research, A 1025 (2022) 166212

Contents lists available at ScienceDirect

Nuclear Inst. and Methods in Physics Research, A

journal homepage: www.elsevier.com/locate/nima

Improving the characterization of fusion in a MuSIC detector by spatial localization

J.E. Johnstone [a,b], Rohit Kumar [a,b], S. Hudan [a,b], R.T. deSouza [a,b,*], J. Allen [c], D.W. Bardayan [c], D. Blankstein [c], C. Boomershine [c], S. Carmichael [c], A. Clark [c], S. Coil [c], S.L. Henderson [c], P.D. O'Malley [c]

[a] Department of Chemistry, Indiana University, 800 E. Kirkwood Ave., Bloomington, IN 47405, USA
[b] Center for Exploration of Energy and Matter, Indiana University, 2401 Milo B. Sampson Lane, Bloomington, IN 47408, USA
[c] Department of Physics, University of Notre Dame, Notre Dame, IN 46556, USA

ARTICLE INFO

Keywords:
MuSIC
Multi-sampling ionization chamber
Trace-matching
Fusion

ABSTRACT

Multi-Sampling Ionization Chambers (MuSIC) provide an efficient means of measuring nuclear reactions with low beam rates (< 10^6 pps). However, in comparison to thin-target measurements, prior measurements using MuSIC detectors all manifest fusion excitation functions with wide error bars in the energy dimension. This uncertainty limits the applicability of these devices in measuring near and sub-barrier fusion cross-sections. Key to overcoming this limitation is spatial localization of the fusion in the detector. By comparing the measured ionization in the MuSIC detector with accurate energy loss calculations the position of the fusion in the detector is determined. The analysis not only provides the desired improvement in energy resolution, but it also allows extraction of the atomic number of the evaporation residues following fusion. The effectiveness of this approach is demonstrated for $^{18}O+^{12}C$ measured with MuSIC@Indiana.

1. Introduction

Reactions of nuclei with exotic neutron-to-proton ratios (N/Z) are a topic of fundamental interest in the fields of both nuclear physics and nuclear astrophysics. Enabling the investigation of this topic is a new generation of radioactive beam facilities [1,2] that promise to make previously inaccessible nuclei available for the first time. Beams of the most exotic N/Z nuclei however, dictated by their short half-lives, are only available at low-intensity. The low-intensity of these radioactive beams suggests a thick-target approach as an effective means for measuring cross-sections. In recent years, active thick-target measurements have gained visibility in low-energy nuclear physics with the increasing use of time-projection chambers [3–8]. Use of these powerful and complex detectors, often rate-limited in their readout, is not warranted for all measurements however. An example of a measurement benefiting from a simpler approach is measurement of the near-barrier fusion cross-section for low-intensity beams. A particularly simple active, thick-target detector suitable for the measurement of fusion cross-sections is a Multi-Sampling Ionization Chambers (MuSIC). MuSIC detectors are intrinsically efficient as they measure multiple points on an excitation function for a single incident beam energy and provide an angle-integrated measurement of the fusion cross-section. These detectors have been demonstrated to be an effective means for measuring fusion using low-intensity beams [9–13]. MuSIC detectors have also been utilized in the measurement of (α, p) and (α, n) reactions [14–16]. Despite these advantages, fusion measurements with MuSIC detectors have to date been subject to an inherent limitation, namely the energy uncertainty associated with each cross-section measured. The present work describes how this limitation is overcome.

In this work the improved simulation and analysis of fusion data from a MuSIC detector, MuSIC@Indiana, is detailed. The measurement of the energy loss of multiple ions enables a better characterization of the detector response. Development of a library of simulated traces is delineated that allows comparison of experimental and simulated traces in a trace-matching analysis. To demonstrate the effectiveness of this approach, the analysis of experimental data for ^{18}O + ^{12}C, measured with MuSIC@Indiana, is presented. The results are compared with data in the literature and the implications of the improved analysis are discussed.

2. Description of a MuSIC detector

MuSIC detectors are transverse-field, Frisch-gridded ionization chambers with segmented anodes [17]. The segmentation of the anode transverse to the beam direction allows the energy loss of a particle traversing the detector to be measured as a function of its position along the beam axis. For a single incident particle the measurement

* Corresponding author at: Department of Chemistry, Indiana University, 800 E. Kirkwood Ave., Bloomington, IN 47405, USA.
E-mail address: desouza@indiana.edu (R.T. deSouza).

https://doi.org/10.1016/j.nima.2021.166212
Received 5 October 2021; Accepted 10 December 2021
Available online 20 December 2021

of the collective ΔE values measured in a MuSIC detector is referred to as a "trace". MuSIC detectors operate best at low-intensities (< 10^6 pps) where the beam rate does not have a significant effect on the performance of the detector gas.

When fusion occurs in the MuSIC detector the increased atomic and mass number of the fusion product results in a sharp increase in the specific ionization along with a decrease in the range as compared to the beam. Consequently, a sharp rise and peak in the trace occurs. Observation of this increased ΔE as compared to ΔE_{Beam} thus provides the ability to deduce that fusion has occurred. From the simplest perspective, fusion events can thus be associated with the anode in which the fusion occurred. Given the atom density of the gas and the number of beam particles incident on that anode the fusion cross-section for each anode is calculated. Along with the cross-section, consideration of the energy lost by the beam prior to the anode allows determination of the energy incident on that anode. In this way, multiple points along an excitation function are simultaneously measured . In this simplest approach of analyzing MuSIC data the fusion cross-section is therefore discretized (binned) based on the anode in which fusion occurs [10,12]. Consequently, the corresponding excitation function has error bars in the energy dimension corresponding to the energy loss of the beam in a single anode. These broad energy error bars also diminish the observation of fine structure in the excitation function of the reaction being studied [18]. Typically, no additional information about the evaporation residues (atomic number, energy, etc.) is reported. To move beyond this simple approach we propose to utilize the entire information contained in a MuSIC trace.

Guided by simulated traces [18] previous MuSIC measurements have extracted reaction cross-sections for (α, p) and (α, n) reactions. Known limitations in the simulation of the traces however restricted the comparison to only a qualitative description. Moreover, describing fusion traces accurately is complicated by the wider range of atomic and mass number of the reaction products as compared to (α, p) and (α, n) reactions. Past simulations of fusion in MuSIC detectors has been hampered but the aforementioned difficulties preventing the extraction of more detailed information on the fusion [10].

3. Conceptual framework

As a beam particle traverses the detector it deposits an energy ΔE on an anode corresponding to:

$$\Delta E = \int_{x_1}^{x_2} \left(\frac{dE}{dx}\right)_{Beam} dx$$

where x_1 and x_2 represent the upstream and downstream edges of an anode respectively. When low-energy fusion occurs, amalgamation of the projectile and target nuclei produces a compound nucleus that de-excites via neutron and charged-particle evaporation on the timescale of 10^{-20} s. The resulting evaporation residue (ER) causes ionization in the gas based on its characteristic specific ionization. For the anode on which the fusion occurs at position x, the energy deposit becomes:

$$\Delta E = \int_{x_1}^{x} \left(\frac{dE}{dx}\right)_{Beam} dx + \int_{x}^{x_2} \left(\frac{dE}{dx}\right)_{ER} dx$$

By simulating traces for all possible ERs and comparing these traces with those experimentally observed, some localization of the fusion position can be achieved. This localization reduces the energy uncertainty in the fusion excitation function. It should also allow determination of additional information about the fusion event namely the atomic number and energy of the evaporation residue.

4. Simulation of fusion in MuSIC@Indiana

In order to execute a trace-matching analysis of MuSIC experimental data, it is necessary to accurately simulate MuSIC events for putative ERs. In the approach we have adopted, accurate *in situ* measurement of energy loss for multiple ions in the detector gas together with energy loss calculations provides the necessary reference library for extracting an improved description of fusion. To demonstrate the effectiveness with which the spatial localization of fusion can be achieved the simulation and analysis of a ^{18}O beam at E_{lab} = 55 MeV impinging on CH_4 gas at 150 Torr is examined in order to compare to experimental data [12].

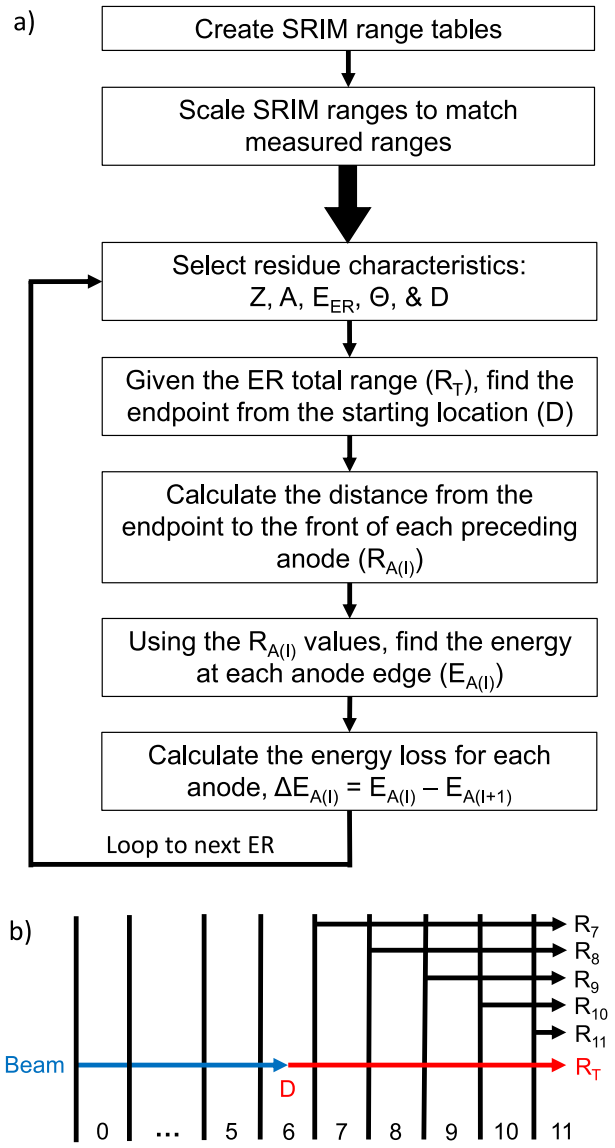

Fig. 1. Panel a: Flowchart for the simulation of fusion events for MuSIC@Indiana events. Panel b: Schematic diagram illustrating the simulation of a fusion event. The location of fusion inside the detector is given as D and relevant distances from the fusion location are given as $R_A(I)$.

The flowchart for simulating MuSIC@Indiana events is shown in Fig. 1a. In the first step, range tables are created using the energy loss program SRIM [19], with a unique range table for both the beam as well as each possible ER. For each ion calculated, the energy spans the interval from 1 keV to 100 MeV with consecutive energies differing by less than 15%. Within this energy range, to interpolate between calculated values of the energy a spline fit is employed. Before explaining the remainder of the steps in the flowchart (Fig. 1a), as the range determination is a critical element in the analysis, it is necessary to describe the procedure for determining the range of different ions in further detail.

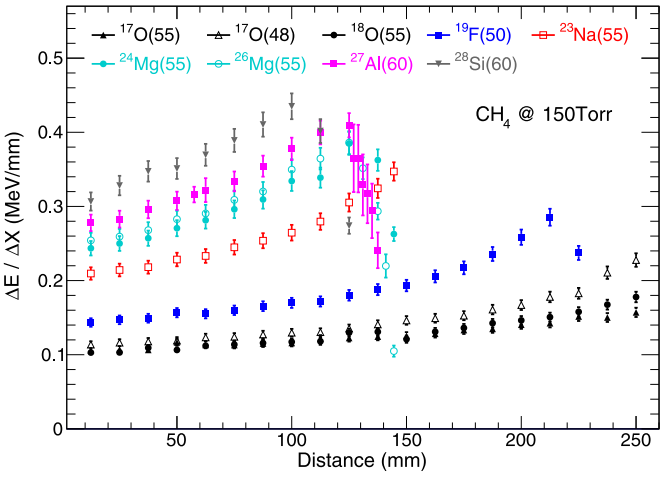

Fig. 2. Measured energy loss for several isotopes including potential residues. Listed along each isotope is the incident energy in MeV.
Source: Figure taken from [12].

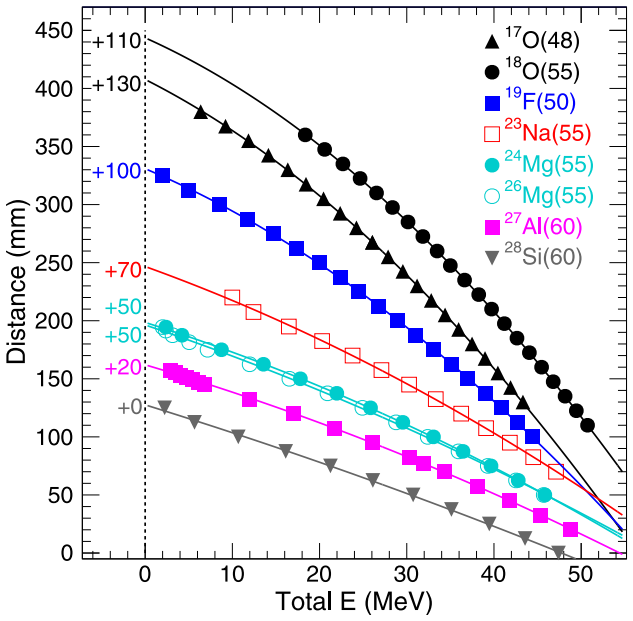

Fig. 3. The distance from the front of MuSIC@Indiana as a function of the energy measured by the SBD for all measured ions. Listed in parenthesis is the incident energy in MeV. For clarity the curves are vertically offset by the numbers indicated on the left.

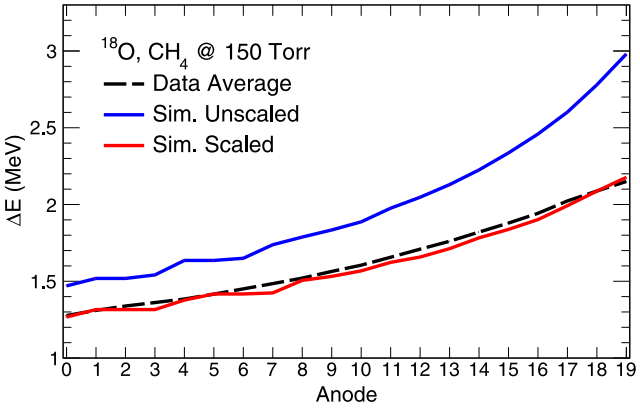

Fig. 4. The average experimental beam trace (dashed black line) is presented along with a simulated beam trace before (solid blue line) and after (solid red line) scaling the SRIM ranges. (For interpretation of the references to color in this figure legend, the reader is referred to the web version of this article.)

It is well established that energy loss values in SRIM when compared to other energy loss programs or experimental data often exhibit uncertainties of approximately 10% [10,18]. Other energy loss programs also exhibit comparable uncertainties. To minimize this uncertainty, the range of specific ions in the detector gas were measured. These measured ranges were used, as described below, to scale the calculated SRIM ranges as indicated in the second step of Fig. 1a. Low-intensity beams of ions with $8 \leq Z \leq 14$ were accelerated by the 10 MV tandem accelerator at Notre Dame University and impinged on MuSIC@Indiana. In addition, multiple isotopes of both oxygen and magnesium nuclei were also measured to quantify the isotopic impact on energy loss. To measure the $\Delta E/\Delta x$ a silicon surface barrier detector was attached to a linear-motion vacuum feedthrough and inserted into the active area of MuSIC@Indiana. Further details of these measurements are given in [12]. The results of these measurements are presented in Fig. 2. A clear separation of the energy loss curves for the different Z is observed in Fig. 2, while the separation between different isotopes of the same element is, as expected, significantly smaller.

To extract the experimental range of each isotope, the correlation between measured energy and position in the detector is plotted in Fig. 3. The distance is taken relative to the upstream edge of the detector. For each nuclide the measured correlation is fit with a second degree polynomial. As can be seen in Fig. 3, the parameterization provides a good description of the data even for all ions independent of whether they stopped in the detector gas. These fits are extrapolated to the stopping point, e.g. zero remaining energy, to find each isotope's experimental range. The relationship between the SRIM range and the experimental range is defined as:

$$R_{EXP} = Slope * R_{SRIM}$$

Since for a ion with zero energy, the range must be zero. For a given nuclide, the slope is defined by the point (R_{SRIM}, R_{EXP}) at the upstream edge of the detector. The slope for all measured nuclides is given in Table 1. For any nuclide in the simulation without an experimentally measured range, the SRIM range is scaled using a slope taken as the average slope of all measured nuclides.

The energy loss for the beam in MuSIC@Indiana is shown in Fig. 4. The average experimental beam trace (dashed black line) is compared to the simulated beam trace from SRIM (solid blue line). The simulation produces a trace which is systematically 15%–35% higher in ΔE than what is measured by MuSIC@Indiana. After scaling, the simulated beam trace (solid red line) matches the experimental trace to within 4% (≈60 keV) for all anodes, showing the effectiveness of the range scaling.

Table 1
Parameters for scaling SRIM ranges.

Isotope	Slope
^{17}O	1.1905
^{18}O	1.1542
^{19}F	1.1687
^{23}Na	1.1472
^{24}Mg	1.1444
^{26}Mg	1.1368
^{28}Si	1.1803

Once the SRIM ranges have been appropriately scaled for the beam and the residues, the first step in simulating a fusion event is to select the characteristics of the fusion event which will determine the energy loss throughout MuSIC@Indiana. The energy loss for each event is characterized by the ER atomic number (Z), mass number (A), energy

Table 2
ER characteristics used for creating the simulated library.

Z	A_{min}	A_{max}	Θ_{min} (°)	Θ_{max} (°)
10	19	23	0.0	25.0
11	22	26	0.0	20.0
12	23	28	0.0	20.0
13	26	29	0.0	15.0
14	26	29	0.0	15.0

(E_{ER}), and angle (θ), as well as the location at which the simulated fusion occurs (D).

Potential ERs for the reaction of interest, $^{18}O + ^{12}C$, are determined using the statistical decay code evapOR [20]. All potential isotopes with a probability above 0.1% in evapOR are simulated, with the ER characteristics presented in Table 2. The angle of ER emission ranges from Θ_{min} to Θ_{max} with a 5° spacing. Because the ER distributions manifest a narrow range in Θ, its impact on the energy deposit in an anode is negligible. The energies of the ER, E_{ER}, simulated are also guided by evapOR. They are chosen to range from 5 to 45 MeV with a 1 MeV spacing. The location of fusion (D) is simulated as spanning the active detector length (250 mm) in increments of 0.5 mm. Although some less likely events are simulated, this method minimizes the influence of inaccuracies in evapOR on the library.

Once these parameters are assigned for a specific library event, the total range of the ER (R_T) is determined using the range table. The distance from the endpoint to the front of each preceding anode ($R_{A(I)}$) is calculated as illustrated in Fig. 1b. The energy of the ER at the front of each anode ($E_{E(I)}$) can then be determined using these distances and the range table. Lastly, the energy loss over a single anode ($\Delta E_{A(I)}$) is calculated as $\Delta E_{A(I)} = E_{E(I)} - E_{E(I+1)}$. Prior to the point of fusion, D, the energy loss is assigned to be that of simulated beam.

5. Trace-matching analysis for MuSIC data

With the library of simulated traces defined, the procedure for analyzing a fusion event is depicted in the flowchart presented in Fig. 5. From the experimental event data, fusion events are distinguished from un-reacted beam, proton capture, and two-body scattering as published [12]. In essence, a trace is categorized as corresponding to fusion based upon it surpassing a minimum ΔE threshold above ΔE_{Beam} and having a range consistent with an ER. At this point each fusion event is associated with the anode, $A_{Threshold}$, for which the minimum threshold is surpassed. In the present analysis the position of the fusion is localized by comparing the measured MuSIC@Indiana trace to all library events in a "trace-matching" process. The span of ER energies considered is limited by summing the ΔE from $A_{Threshold}$ to A_{19}. Only library events with energies within 3 MeV of this energy are considered. The deviation of the experimental event from a library event is assessed through the calculation of the quantity η^2, defined as:

$$\eta^2 = \sum_{Anodes} (\Delta E^{exp}_{A(I)} - \Delta E^{sim}_{A(I)})^2$$

The library event with the minimum η^2 is identified and subsequently used as a reference for calculating residue characteristics. Each fusion event characteristic (D, Z, E_{ER}, A, and Θ) is calculated to be the average value for all library events within 0.2 of the minimum η^2. In general, traces for library events above $\eta^2_{min} + 0.2$ were observed to deviate consistently from the data trace beyond the level of the detector noise. As such, events with a η^2 greater than 0.2 above η^2_{min} are not included in the calculation of the average D, Z, E_{ER}, and A.

A representative experimental fusion trace (blue) is presented in Fig. 6a, alongside the trace of its associated η^2_{min} library event (red). The η^2_{min} event shows excellent agreement with the data trace. To examine the differences between the two, the deviation of the η^2_{min} library event from the experimental fusion trace is depicted in Fig. 6b as the red line. Its deviation from the data at the peak, anode 7, is ≈ 60 keV well within

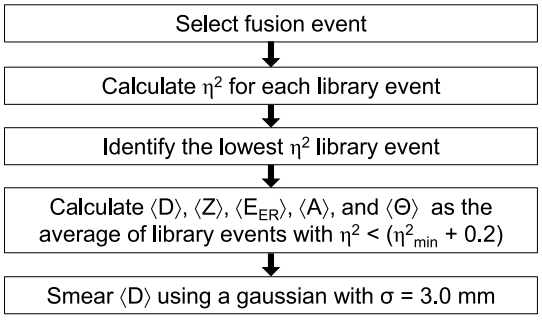

Fig. 5. Flowchart depicting the logic of the trace-matching analysis implemented.

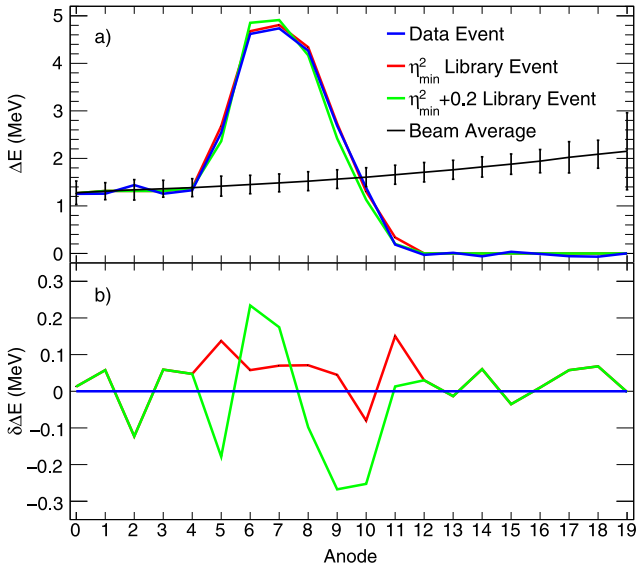

Fig. 6. An experimental MuSIC@Indiana trace with both the library trace of minimum η^2 and the library trace of minimum η^2 + 0.2 is shown in panel a. The average beam behavior is also shown for reference with error bars representing the FWHM of the noise seen in the detector. Panel b shows the deviation of both library traces from the experimental event. (For interpretation of the references to color in this figure legend, the reader is referred to the web version of this article.)

the energy uncertainty of the ΔE signal. A measure of what represents a reasonable deviation is realized by examining the distribution of all beam events represented by the error bars on the average beam trace (black, FWHM ≈ 200 keV) shown in Fig. 6a. In addition, Fig. 6a shows the trace for the library event at η^2_{min} + 0.2 (green). This trace is also in good agreement with the data and is within the uncertainty on the ΔE signal observed during the experiment.

For the data event shown in Fig. 6a, the dependence of the η^2 value as a function of D and each of the ER characteristics Z, E_{ER}, and A is shown in Fig. 7a-d, respectively. Also presented in Fig. 7a-d are the mean and RMS values of each distribution. The width of the D distribution, 0.893 mm, is much smaller than a single anode width of 12.5 mm. This indicates that one can achieve sub-anode resolution on the location of fusion in MuSIC@Indiana. From the value of D the energy at which fusion occurs can be directly calculated allowing a higher granularity determination of the fusion excitation function — one that is not determined by the anode geometry of the detector. As shown in Fig. 7b, the Z distribution is well-defined with most events corresponding to a single Z value. Similarly, Fig. 7c shows a narrow distribution in E_{ER} with all events falling within 0.5 MeV of the average. As observed in the $\Delta E/\Delta x$ measurements presented in Fig. 2, the energy loss has a slight dependence on A. This weak dependence provides a poor discrimination capability for A and is reflected in Fig. 7d by a relatively broad A distribution spanning 4–5 masses.

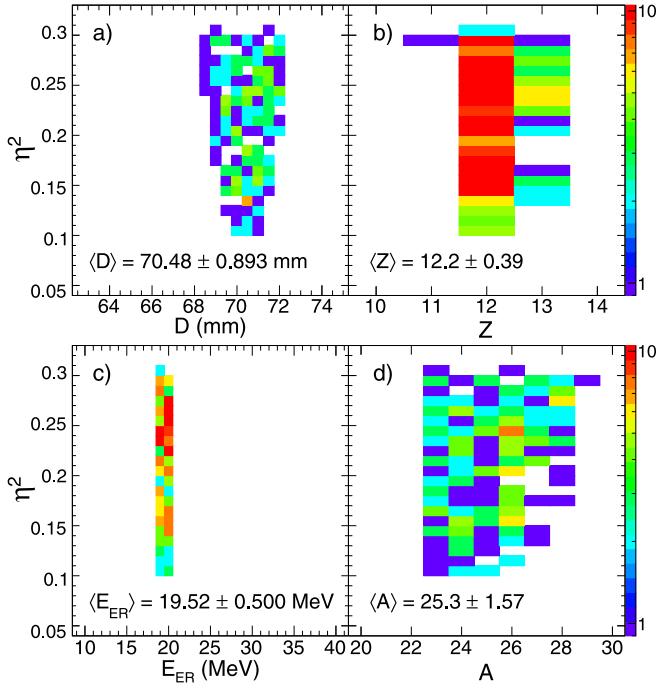

Fig. 7. η^2 distributions for a single data event as a function of the D, Z, E_{ER}, and A are shown in panels a–d, respectively. Each variable is presented with the mean and root mean square values of the distribution.

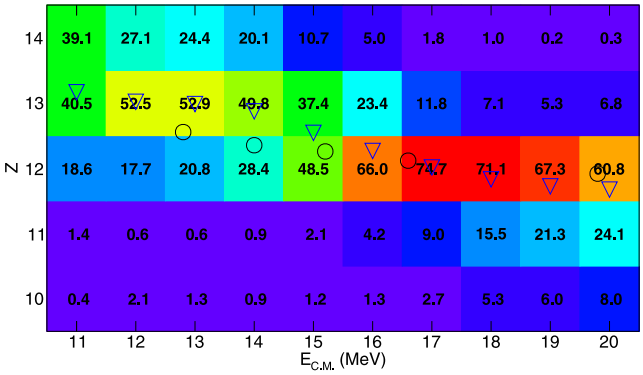

Fig. 8. Fusion evaporation residue Z distribution as a function of $E_{C.M.}$ for ^{18}O + ^{12}C. Numbers indicate the elemental percentage for a given bin in $E_{C.M.}$. The $\langle Z_{ER}\rangle$ from this work is shown as the open triangles while $\langle Z_{ER}\rangle$ from [22] is indicated by the open circles.

The energy loss values in the library do not account for the variation in ΔE experimentally measured due to both the Fano factor of the gas and the electronic noise. This deficiency can be framed in terms of an uncertainty in the extracted value of D. The average D is smeared using a Gaussian distribution centered at the averaged D value with σ_D = 3.0 mm as indicated in the last step of Fig. 5.

6. Results with ^{18} O + ^{12}C MuSIC@Indiana data

The analysis technique described in Section 5 was applied to the ^{18}O + ^{12}C reaction for data collected using MuSIC@Indiana. The experiment was performed at the University of Notre Dame's Nuclear Science Laboratory. A beam of $^{18}O^{6+}$ ions was accelerated by the 10 MV tandem accelerator to E_{lab} = 55 MeV and bombarded MuSIC@Indiana filled with 150 Torr of CH_4. Further experimental details have been previously reported [12].

As demonstrated in Fig. 7b, the trace-matching analysis allows for the extraction of residue Z with high confidence. The experimental Z distribution as a function of $E_{C.M.}$ for ^{18}O + ^{12}C is presented in Fig. 8. A clear trend is observed as a function of $E_{C.M.}$, with Z ≤ 12 dominating the distribution at higher energies and a shift to Z ≥ 13 dominating at lower energies. This trend is consistent with a previous investigation of the α-emission cross-section from the compound nucleus [21]. A near 100% probability for α-emission at $E_{c.m.}$ = 14 MeV was observed, with the probability falling off substantially for lower incident energies [21]. The trend observed in Fig. 8 indicates good agreement with these results. The Z distribution as a function of $E_{C.M.}$ has been previously reported [22]. The $\langle Z_{ER}\rangle$ reported in [22] is shown in Fig. 8 as the open circles. In comparison, the $\langle Z_{ER}\rangle$ for the current work is portrayed as the open triangles. The good agreement of the measured $\langle Z_{ER}\rangle$ in the current work as compared to prior measurements [21,22] suggests that the current analysis is correctly identifying the $\langle Z_{ER}\rangle$.

Presented in Fig. 9a are the results of the trace-matching analysis binned at the one-anode level (ΔD = 12.5 mm), alongside the same data set as analyzed according to the simpler analysis of [12]. One should note that in both cases the represented error bars in σ_F are entirely statistical and the error bars in $E_{C.M.}$ are ≈800 keV. All points on the two excitation functions agree within the error bars and no systematic trend is observed. The minor differences between the two analyses are due to the reshuffling of events for which fusion occurs near an anode edge. In the previous analysis [12], a threshold must be set for each anode which designates an event as being fusion in that anode. This threshold is dependent on the noise in the detector. As such, fusion events which occur deep in an anode may not be identified as fusion-like until the subsequent anode. For the entire excitation function this is a small effect as each anode gains events from the preceding anode and loses events to the following anode. This results in a "smoothing" of the excitation function as the anode edges do not provide a sharp cutoff for binning in the simple analysis. In contrast, the present trace-matching analysis properly identifies the location of these events near an anode edge and assigns them to the correct energy in the excitation function.

The same trace-matching analysis is presented in Fig. 9b binned at the half-anode level (ΔD = 6.25 mm). Increasing the number of points by a factor of two reduces the energy error bars by a factor of two, ≈400 keV. Correspondingly, on average each datapoint has half the statistics, which only increases the error bars in σ_F by a factor of ≈1.4. As the uncertainty in both energy and cross-section are relevant to the accurate determination of the fusion excitation function, this significant improvement in energy uncertainty at the cost of a modest worsening in the cross-section determination is an overall improvement in the determination of the excitation function. Further reduction in the energy uncertainties evident in Fig. 9b are not warranted given the statistical uncertainties of the present measurement. Overall, this excitation function also matches the results from [12]. Some structures appear to be emerging, notably small peaks at $E_{C.M.}$ ≈ 15.3 and 16.5 MeV.

To better understand the nature of these structures, this excitation function is plotted against literature data in Fig. 10. The literature data matches the present data well, in particular because of the non-smooth behavior observed for the current work. Below $E_{C.M.}$ = 14 MeV, this work is in good agreement with all three literature datasets. At energies above $E_{C.M.}$ = 15 MeV where the non-smooth behavior is most pronounced, the present work agrees with Heusch and maps out oscillations which are common in light fusing systems [23–25]. Inspection of Heusch together with the present data indicates the presence of oscillations most prominently a broad structure between 16 and 18 MeV. While the Heusch data is consistent with these oscillations, taken on its own it does not have enough definition of the excitation function in this energy range to observe these structures definitively. This comparison of the literature and the MuSIC@Indiana data highlights an inherent advantage of measuring fusion with a MuSIC detector and employing the present analysis. With this analysis, the energies at which fusion

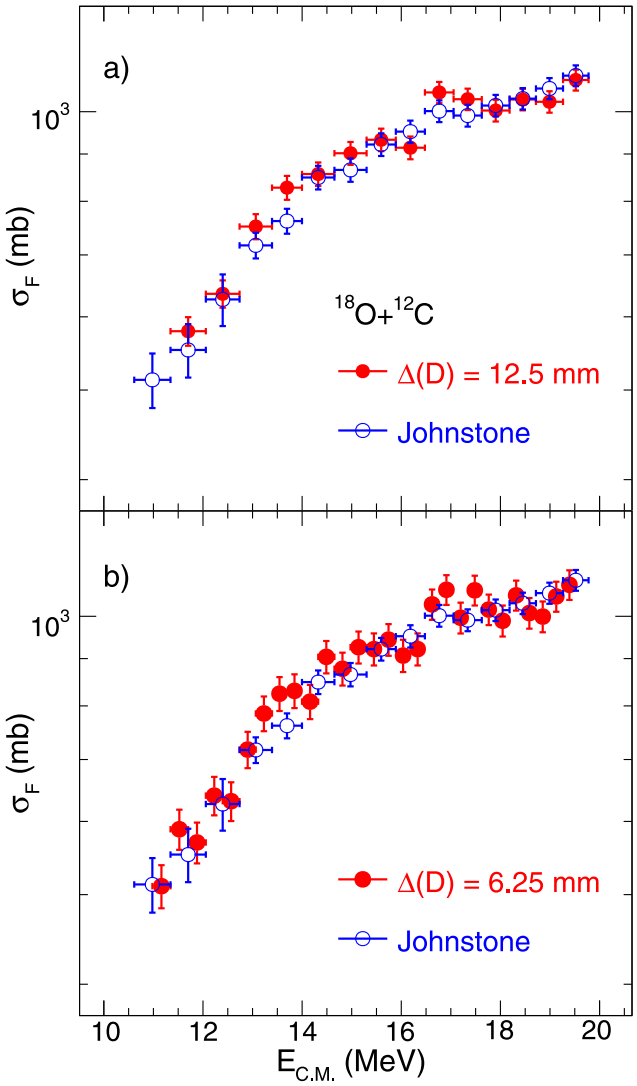

Fig. 9. The measured fusion excitation function of $^{18}O + ^{12}C$ extracted using the trace-matching analysis technique together with the published excitation function of the same data from [12]. The extracted excitation function is shown binned at the 1-anode (a) and half-anode (b) levels.

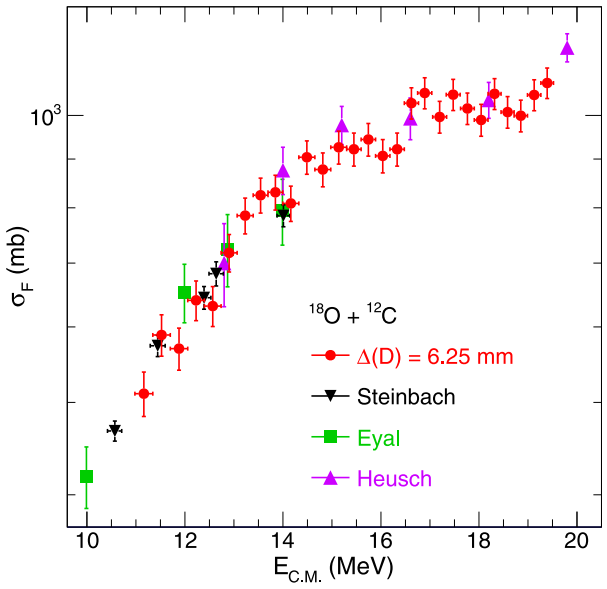

Fig. 10. Comparison of the high resolution fusion excitation function of $^{18}O + ^{12}C$ obtained with the trace-matching analysis technique with the thin-target data sets of Steinbach [26], Eyal [27], and Heusch [22].

is measured are decoupled from the anode segmentation, effectively providing a measurement of the fusion excitation function that is continuous in energy. The current analysis also underscores the importance of improving the energy resolution of an excitation function for locating narrower structures. While this work provides evidence for oscillatory structure in the $^{18}O + ^{12}C$ excitation function, the magnitude of these oscillations is comparable to the present statistical uncertainties in the measured cross-section. As such, further measurements which acquire higher statistics should be performed in order to confirm these results.

7. Conclusions

A new approach for analyzing fusion data from a MuSIC detector is presented. This analysis which relies on matching the measured ΔE in a MuSIC trace with simulated energy loss curves results in the extraction of a high resolution fusion excitation function. A critical element in this analysis is development of an energy loss library which necessitated accurate energy loss measurements for the ions of interest. Using a library for $^{18}O + ^{12}C$ a trace-matching analysis of experimental data was performed. As a result of this analysis the evaporation residue Z distribution was obtained along with a localization of the fusion position within an anode. This localization of the fusion position allowed construction of a high resolution fusion excitation function with significantly reduced energy error bars. The final excitation function obtained has energy error bars which are comparable to those obtained for thin-targets for low-intensity beams.

The trace-matching analysis developed decouples the excitation function measured by a MuSIC detector from the detector anode geometry. This decoupling enables the energy interval over which the cross-section is measured to be chosen after the data collection allowing the identification of structures in an excitation function. In the present case of $^{18}O + ^{12}C$, the improved energy resolution provides evidence for an oscillatory structure previously unidentified in the literature. This result suggests the potential of future fusion MuSIC measurements to examine the influence of structure on near-barrier fusion.

Declaration of competing interest

The authors declare that they have no known competing financial interests or personal relationships that could have appeared to influence the work reported in this paper.

Acknowledgments

The authors would like to thank Indiana University Mechanical Instrument Services and Electronic Instrument Services in the Department of Chemistry for their help in constructing the MuSIC@Indiana detector. This work was supported by US Department of Energy under Grant No. DE-FG02-88ER-40404. The research was also sponsored by National Science Foundation (NSF), USA Grant No. PHY-2011890 and by the University of Notre Dame, USA.

References

[1] G. Bollen, AIP Conf. Proc. 1124 (2010) 432.
[2] P. Dolegieviez, et al., Status of the SPIRAL2 Project, Tech. rep., 2019.
[3] M. Cwoik, et al., IEEE Trans. Nucl. Sci. 52 (2005) 2895.
[4] J.J. Kolata, et al., Nucl. Instrum. Methods A 830 (2016) 82.
[5] Y. Ayyad, et al., Nucl. Instrum. Methods A 954 (2020) 161341.
[6] M. Gai, et al., Nucl. Instrum. Methods A 954 (2020) 161779.
[7] E. Koshchiy, et al., Nucl. Instrum. Methods A 957 (2020) 163398.

[8] D. Bazin, et al., Prog. Part. Nucl. Phys. 114 (2020) 103790.
[9] P.F.F. Carnelli, et al., Phys. Rev. Lett. 112 (2014) 192701.
[10] P.F.F. Carnelli, et al., Nucl. Instrum. Methods A 799 (2015) 197–202.
[11] B.W. Asher, et al., Phys. Rev. C 103 (2021) 044615.
[12] J.E. Johnstone, et al., Nucl. Instrum. Methods A 1014 (2021) 165697.
[13] B.W. Asher, et al., Eur. Phys. J. A. 57 (2021) 272.
[14] M.L. Avila, et al., Phys. Rev. C 94 (2016) 065804.
[15] R. Talwar, et al., Phys. Rev. C 97 (2018) 055801.
[16] B.W. Asher, et al., Nucl. Instrum. Methods A 1014 (2021) 165724.
[17] W.B. Christie, et al., Nucl. Instrum. Methods A 255 (1987) 466–476.
[18] M.L. Avila, et al., Nucl. Instrum. Methods A 859 (2017) 63–68.
[19] J.F. Ziegler, et al., Nucl. Instrum. Methods Phys. Res. B 268 (2010) 1818–1823.
[20] N.G. Nicolis, J.R. Beene, unpublished.
[21] J. Vadas, et al., Phys. Rev. C 92 (2015) 064610.
[22] B. Heusch, et al., Phys. Rev. C 26 (1982) 542.
[23] P. Sperr, et al., Phys. Rev. Lett. 37 (1976) 321.
[24] I. Tserruya, et al., Phys. Rev. C 18 (1978) 1688.
[25] D.G. Kovar, et al., Phys. Rev. C 20 (1979) 1305.
[26] T.K. Steinbach, et al., Phys. Rev. C 90 (2014) 041603.
[27] Y. Eyal, et al., Phys. Rev. C 13 (1976) 1527.